1174 *Biochemistry* **2011,** *50,* 1174–1183
DOI: 10.1021/bi101689b

BIOCHEMISTRY
including biophysical chemistry & molecular biology
Article

Light-Induced Movement of the LOV2 Domain in an Asp720Asn Mutant LOV2−Kinase Fragment of *Arabidopsis* Phototropin 2[†]

Yuki Takayama,[‡,§] Masayoshi Nakasako,*[,‡,§] Koji Okajima,[∥] Aya Iwata,[‡] Sachiko Kashojiya,[∥] Yuka Matsui,[‡,§] and Satoru Tokutomi*[,∥]

[‡]*Department of Physics, Faculty of Science and Technology, Keio University, 3-14-1Hiyoshi, Kohoku-ku, Kanagawa 223-8522, Japan,* [§]*The RIKEN Harima Institute/SPring-8, 1-1-1 Kouto, Mikaduki, Sayo, Hyogo 679-5148, Japan, and* [∥]*The Department of Biological Science, Osaka Prefecture University, 1-1 Gakuen-cho, Sakai, Osaka 599-8531, Japan*

Received October 20, 2010; Revised Manuscript Received January 10, 2011

ABSTRACT: Phototropin, a blue-light receptor protein of plants, triggers phototropic responses, chloroplast relocation, and opening of stomata to maximize the efficiency of photosynthesis. Phototropin is composed of two light−oxygen−voltage sensing domains (LOV1 and LOV2) that absorb blue light and a serine/theroine kinase domain responsible for light-dependent autophosphorylation leading to cellular signaling cascades. Although the light-activated LOV2 domain is primarily responsible for subsequent activation of the kinase domain, it is unclear how conformational changes in the former transmit to the latter. To understand this molecular mechanism in *Arabidopsis* phototropin 2, we performed small-angle X-ray scattering analysis on a fragment composed of the LOV2 and kinase domains, which contained an Asp720Asn mutation that led to an absence of ATP binding activity. The scattering data were collected up to a resolution of 25 Å. The apparent molecular weight of the fragment estimated from scattering intensities demonstrated that the fragment existed in a monomeric form in solution. The fragment exhibited photoreversible changes in the scattering profiles, and the radii of gyration under dark and blue-light irradiation conditions were 32.4 and 34.8 Å, respectively. In the dark, the molecular shape restored from the scattering profile appeared as an elongated shape of 110 Å in length and 45 Å in width. The homology modeled LOV2 and kinase domains could be fitted to the molecular shape and appeared to make slight contact. However, under blue-light irradiation, a more extended molecular shape was observed. The changes in the molecular shape and radius of gyration were interpreted as a light-dependent positional shift of the LOV2 domain of approximately 13 Å from the kinase domain. Because the region connecting the LOV2 and kinase domains was categorized as a naturally unfolded polypeptide, we propose that the light-activated LOV2 domain triggers conformational changes in the linker region to separate the LOV2 and kinase domains.

Light-sensing systems in higher plants comprise photoreceptor proteins that convert visible light stimuli into biological signals, which propagate through cellular signal transduction systems regulating developmental and cell motility processes (*1*, *2*). Phototropin (phot), which was first identified as a photoreceptor for phototropic responses (*3*−*5*), is now known to regulate cellular actions, such as chloroplast relocation (*6*−*8*) and opening of stomata (*9*), that maximize the efficiency of photosynthesis. Most plants possess two isoforms of phot, designated phot1[1] and phot2 (*4*, *10*). In *Arabidopsis thaliana*, phot1 and phot2 redundantly regulate the opening of stomata (*9*) and also share phototropic responses and photoaccumulation of chloroplasts depending on the fluence rate of blue light (*8*), whereas only phot2 mediates the photoavoidance response in chloroplast relocation (*7*).

Arabidopsis phot2 comprises 915 amino acid residues and two prosthetic flavin mononucleotide (FMN) molecules (*4*) (Figure 1A). The N-terminal half of the protein folds into a pair of FMN-binding light−oxygen−voltage sensing domains (LOV1 and LOV2) (*11*, *12*), forming a subset of the Per-ARNT-Sim superfamily, which act as protein−protein interaction modules (*13*). The C-terminal half of phot2 is a Ser/Thr kinase domain belonging to the AGC family (cAMP-dependent protein kinase, cGMP-dependent protein kinase, and phospholipid-dependent protein kinase C) (*14*). In *Arabidopsis* phot1, the phosphorylation of the well-conserved Ser residue in the activation loop (A-loop) of the kinase domain represents a key process in light-induced signal transduction (*15*, *16*).

In phots, each LOV domain noncovalently binds one FMN chromophore in the dark. Upon blue-light irradiation, the LOV

[†]This research was supported by Grants-in-Aid from the Ministry of Education, Culture, Sports, Science and Technology to M.N. (15076210, 20050030, and 22018027) and S.T. (17084008 and 1081000118) and from the Japanese Society for the Promotion of Science to M.N. (1920402 and 22244054).

*To whom correspondence should be addressed. M.N.: phone, +81-45-566-1679; fax, +81-45-566-1672; e-mail, nakasako@phys.keio.ac.jp. S.T.: phone, +81-72-254-9841; fax, +81-72-254-9841; e-mail, toxan@b.s.osakafu-u.ac.jp.

[1]Abbreviations: A-loop, activation loop of kinase; AI-loop, activation loop in the kinase domain of *Arabidopsis* phototropin 2 with amino acid insertion; DLS, dynamic light scattering; FMN, flavin mononucleotide; LOV, light−oxygen−voltage sensing; M_w, molecular weight; NMR, nuclear magnetic resonance; P2L2K, fragment containing the LOV2 and kinase domains of *Arabidopsis* phototropin 2; P2LOV2, LOV2 domain of *Arabidopsis* phototropin 2; P2STK, kinase domain of *Arabidopsis* phototropin 2; PCR, polymerase chain reaction; PDB, Protein Data Bank; phot1, phototropin 1; phot2, phototropin 2; R_g, radius of gyration; SAXS, small-angle X-ray scattering; SDS−PAGE, sodium dodecyl sulfate−polyacrylamide gel electrophoresis; SH2, Src homology 2; SH3, Src homology 3.

 Published on Web 01/11/2011

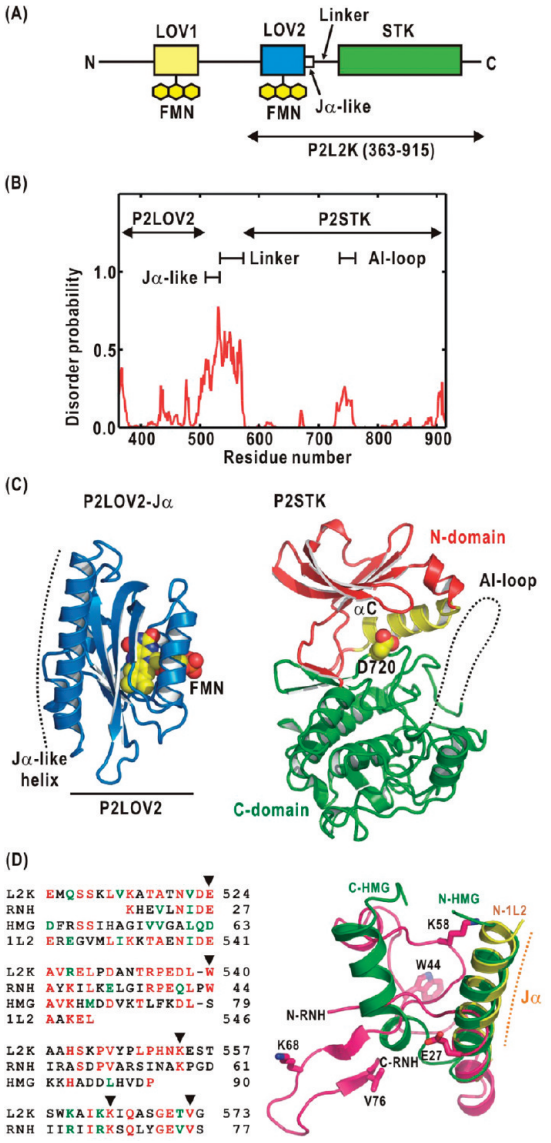

FIGURE 1: (A) Schematic illustration of the domain organization in *Arabidopsis* phot2. The P2L2K region (residues 363−915) used in this study is denoted with an arrow. (B) Disorder probability (*34*) calculated for the P2L2K fragment in panel A plotted vs residue number. Arrows and bars indicate the regions of the P2LOV2 domain (residues 388−504), Jα-like region (residues 505−529), linker region (residues 502−573), P2STK domain (residues 574−864), and AI-loop (residues 753−765). (C) Homology modeled structures of P2LOV2 together with the Jα-like region (P2LOV2-Jα) and P2STK, as illustrated by ribbon models. The P2LOV2-Jα model is colored blue, and FMN is denoted by the atom-colored CPK model. The Jα region in the P2LOV2-Jα model is denoted with a dotted line. In P2STK, the structurally and functionally important segments are colored differently: N-terminal domain (N-domain, red), C-terminal domain (C-domain, green), and helix αC (yellow). AI is drawn as an optional loop with a dotted line. Residue Asp720 shown in the CPK model indicates the point mutation site of P2L2K. This panel was prepared using PyMol (*56*). (D) The left panel shows a sequence alignment for the linker region of P2L2K and segments from an RNA polymerase (abbreviated as RNH) (*41*), hemoglobin (HMG) (*42*), and the Jα helix of the *Avena* phot1 LOV2 domain (1L2) (*20*). The residues identical with those of P2L2K are colored red, and homologous residues are colored green. The right panel shows the superimposition of the ribbon model crystal structures of HMG (green) and RNH (red) on the Jα helix of the *Avena* phot1 LOV2 domain (yellow). Side chains of residues of RNH denoted with triangles in the sequence alignment are shown as atom-colored stick models. The Jα regions of the *Avena* phot1 LOV2 domain are denoted with a dotted line.

domain undergoes a photoreaction cycle through the formation and breakage of a cysteinyl adduct between the FMN and an invariant cysteine residue (*17*, *18*). Adduct formation induces a tilt of the isoalloxazine ring of FMN and reorganization of the hydrogen bond network around the ring (*19*, *20*). These conformational changes in the protein moiety of the LOV domain are assumed to cause blue-light-enhanced autophosphorylation of the kinase domain. Despite the similarities in their structures and photoreaction cycles, LOV1 and LOV2 domains have distinct roles in the structures and functions of phots (*21*).

The LOV1 domains of phot1 and phot2 are thought to act structurally as a dimerization site (*22*, *23*). While LOV1 domain photochemistry is essentially dispensable for phot1 function (*21*), this domain is thought to regulate sensitivity to blue light and induce complementation of phototropism in phot2 (*24*). The LOV2 domain is responsible for the autophosphorylation of the kinase domain and is indispensable for the signal transduction mediated by phot1 and phot2 (*21*). For example, the LOV2 domains of both phot1 and phot2 play essential roles in phototropism and leaf expansion (*25*). The recombinant phot2 LOV2 domain inhibits the activity of the phot2 kinase domain in the dark, although the inhibition is suppressed by blue light (*24*). The *Avena* phot1 LOV2 domain has an amphipathic α-helix, Jα, which displays light-induced conformational changes, a folding−unfolding transition, and dissociation from the LOV2 domain (*20*, *26*, *27*). The *Arabidopsis* phot2 LOV2 domain is assumed to have a similar helix structure, which displays structural changes similar to those of phot1 LOV2 Jα (*28*). The conformational changes are considered to either directly or indirectly propagate to the kinase domain, to liberate the kinase domain from the inhibitory effect of the LOV2 domain (*29*). While the evidence regarding light-induced local conformational changes has been collected during spectroscopic studies, little structural information about the relative arrangements and interactions of the LOV2 and kinase domains in phot molecules both in the dark and upon photoactivation is available.

In this study, we conducted small-angle X-ray scattering (SAXS) analyses on a fragment of *Arabidopsis* phot2 (P2L2K, residues 363−915), which included the LOV2 domain (P2LOV2, residues 388−504) with a C-terminal extension (Jα-like region, residues 505−529) homologous to the Jα helix of the *Avena* phot1 LOV2 domain and the kinase domain (P2STK, residues 574−864) (Figure 1A). The two functional domains are connected by the linker region (residues 530−573). In the kinase domain of this P2L2K, an Asp720Asn mutation was introduced to eliminate its binding affinity for Mg-ATP. Although we overexpressed wild-type P2L2K, the enzymes exhibited different degrees of phosphorylation. It was difficult to purify separately the enzymes to the amount required in the SAXS study. In contrast, mutated P2L2K was purified in a sufficient amount for X-ray studies and was suitable for studying the intramolecular events occurring after the light activation of P2LOV2 and before substrate binding in P2STK. On the basis of the structural parameters, molecular shapes from the SAXS data, and homology models of P2LOV2 and P2STK, we here discuss the molecular mechanism of how light-induced P2LOV2 activates P2STK.

MATERIALS AND METHODS

Purification of Recombinant P2L2K. The overexpression and purification were conducted according to the protocols used for a LOV2−kinase fragment of phot1 (K. Okajima et al.,

manuscript submitted for publication) with the following modifications. The coding region of the *Arabidopsis* P2L2K gene was amplified from the pGEX-phot2 LOV2-kinase vector (*24*) by the PCR method with *Pfu* DNA polymerase (Stratagene) and synthesized primers (5′-GAAAGAATTCATGGAGAGGCCAAGAG-3′ and 5′-GTTTCTCGAGTTAGAAGAGGTCAATGTCCA-AGTCCGTAGAGTTCACAAGCAC-3′). The PCR-amplified product was excised with *Nde*I and *Xho*I and inserted into a pET28a plasmid vector (Novagen) to allow the expression of P2L2K with an N-terminal histidine tag, which was composed of 20 residues, including six histidine residues. Site-directed mutagenesis of the Asp720Asn mutant was performed using the PCR-based site-directed mutagenesis protocol reported previously (*24*). The Asp720Asn mutation was verified through DNA sequencing with a CEQ2000XL DNA analysis system (Beckman Coulter).

Asp720Asn mutant P2L2K was overexpressed in an *Escherichia coli* JM109 strain, which was transformed by the plasmid vector. The strain was grown at 310 K in LB medium containing 30 μg/mL kanamycin for 6 h and then incubated in the presence of 0.02 mM isopropyl β-D-thiogalactopyranoside for 24 h at 293 K in the dark. The purification procedures were conducted at 273−277 K under a dim red light. Harvested bacteria were lysed by sonication in a buffer containing 20 mM HEPES-NaOH, 100 mM NaCl, 10% (w/v) glycerol, and 1 mM phenylmethanesulfonyl fluoride (pH 7.5). The supernatant obtained by a centrifugation of the lysate was mixed with a Ni-chelate resin (Ni-Sepharose High Performance, GE healthcare). P2L2K was eluted from the resin with a buffer containing 500 mM imidazole, 100 mM NaCl, 10% (w/v) glycerol, and 20 mM HEPES (pH 7.5). Further purification by column chromatography was performed using an AKTA prime system (GE healthcare). The P2L2K fractions eluted with imidazols were purified via size exclusion column chromatography (Superdex 200pg, GE healthcare) with a buffer containing 100 mM NaCl, 10% (w/v) glycerol, 1 mM EGTA, and 20 mM Tris-HCl (pH 7.8). After being desalted, the eluted P2L2K fractions were purified using an anion-exchange RESOURCE Q column (GE healthcare) equilibrated with a buffer containing 10% (w/v) glycerol and 20 mM Tris-HCl (pH 7.8). The P2L2K fractions, which were eluted with a linear gradient from 50 to 350 mM NaCl, were desalted again and applied to a cation-exchange RESOURCE S column (GE healthcare) equilibrated with a buffer containing 10% (w/v) glycerol and 20 mM Tris-HCl (pH 7.8). We used the same linear gradient that was used during anion-exchange chromatography. The purity of P2L2K fractions in each step was examined by sodium dodecyl sulfate−polyacrylamide gel electrophoresis (SDS−PAGE).

Purified P2L2K was concentrated by ultrafiltration in a 20 mM HEPES buffer containing 200 mM NaCl and 10% (w/v) glycerol (pH 7.5). A 0.5 mg/mL P2L2K solution after centrifugation (100000*g* for 30 min at 277 K) showed a monodispersive property in a dynamic light scattering (DLS) measurement using a Zetasizer Nano (Malvern Instruments). We estimated the fluid dynamic diameter of P2L2K to be 97.8 ± 0.2 Å from the time correlation function of the fluctuation in the measured scattering intensity.

Measurements of UV−Visible Absorption Spectra and Dark Reversions of P2L2K from a Cysteinyl Adduct State. The absorption spectra of P2L2K under blue-light illumination and the time course of absorption changes during thermal decay from the cysteinyl adduct state to the dark-adapted state were measured at 293 K using a U-3310 spectrophotometer (Hitachi, Tokyo, Japan). P2L2K solutions at a concentration of 37 μM in 20 mM HEPES, 500 mM NaCl, 1 mM EDTA, and 10% (w/v) glycerol (pH 7.5) were assessed after centrifugation at 100000*g* for 30 min at 277 K. A blue photodiode illuminator (λ_{max} = 460 nm) was used for the light activation of P2L2K at a fluence rate of 20−190 μM m^{-2} s^{-1}. The time courses of absorption changes under blue-light illumination at a fluence rate of 190 μM m^{-2} s^{-1} and in successive darkness were monitored at 447 nm.

SAXS Measurement. SAXS data were collected at beamline BL45XU of SPring-8 using an R-axis IV^{++} Imaging-Plate detector (Rigaku, Tokyo, Japan). The X-ray wavelength was tuned to 0.9000 Å; the camera distance was set at 1516.5 mm, and the exposure time was 60 s. All measurements were performed using a sample cell with quartz windows with a thickness of 0.01 mm and a path length of 3.0 mm. The temperature of the samples was maintained at 293 K.

In a preliminary SAXS experiment for a 2 mg/mL P2L2K solution, we observed profiles with severe aggregation in the small-angle region (Figure S1A of the Supporting Information). On the basis of our experience in the SAXS study of pea phytochrome A (*30*), ultracentrifugation was thought to be effective for the elimination of aggregation from concentrated sample solutions for SAXS measurements. SAXS was sensitive to the aggregation of proteins; a centrifugal force stronger than that applied for samples used in the DLS and absorption measurements was necessary to remove aggregation components. Thus, prior to the SAXS measurements, the concentrated P2L2K sample was centrifuged at 300000*g* for 1 h using a himac CP 85β instrument (Hitachi). The centrifugal force and period were enough to prepare >2 mg/mL monodispersive P2L2K solutions as judged from the SAXS profiles (Figure S1B of the Supporting Information).

SAXS profiles of P2L2K were collected in the concentration range from 0.5 to 3.2 mg/mL. For each sample solution, a set of measurements was sequentially performed in the dark, under blue-light irradiation, and again in the dark. Samples were irradiated with a filtered light-emitting diode array placed 100 mm from the sample. The filtered light had a wavelength maximum of 480 nm and a half-bandwidth of 40 nm (4515C, Nakagawa Chemicals). The fluence rate at the sample position was 450 μM m^{-2} s^{-1}. When SAXS profiles were recorded under blue-light irradiation, the samples were preirradiated for 5 min before being exposed to X-rays to ensure a high population of light-activated P2L2K. After X-ray exposure under blue-light irradiation, the samples were kept in the dark for 5 min. SAXS profiles were then collected again in the dark. SAXS data of hen egg white lysozyme [M_w = 14.3K (Wako Chemical Industry, Osaka, Japan)] were also collected as a reference for determining the apparent M_w of P2L2K. The occurrence of minimal radiation damage to all samples was confirmed by the stabilities of successively recorded SAXS profiles, absorption spectra, and SDS−PAGE patterns after X-ray exposure.

SAXS Analysis. The two-dimensionally recorded SAXS patterns were reduced to one-dimensional profiles after subtraction of the background scattering of the buffer solution. SAXS profiles in the small-angle region were analyzed by Guinier's approximation (*31*). At a scattering vector S, the scattering intensity $I(S,C)$ of a protein solution at a concentration C was approximated by the forward scattering intensity $I(S=0,C)$ and the radius of gyration $R_g(C)$ as

$$I(S,C) = I(S=0,C)\exp[-4\pi^2/3R_g(C)^2S^2],\ S = 2\sin\theta/\lambda$$

where 2θ is the scattering angle and λ is the X-ray wavelength.

Under dilute conditions, the concentration dependencies of $I(S=0,C)$ and $R_g(C)^2$ were approximated as

$$KC/I(S=0,C) = 1/M_w + 2A_2C$$

$$R_g(C)^2 = R_g(C=0)^2 - B_{if}C$$

where K is a constant, M_w is the apparent molecular weight of the protein, A_2 is the second virial coefficient, and B_{if} reflects interprotein interactions (*31*). Attractive interprotein interactions result in a negative A_2, while repulsive interactions give a positive value. The sign of B_{if} is identical to that of A_2. Assuming the partial specific volume of 0.74 cm^3/g for ssoluble proteins, we can determine the apparent M_w of a soluble protein using $I(S=0, C=0)$ of a reference protein (lysozyme) with a known M_w.

The $S < 0.015$ $Å^{-1}$ intensity profiles were extrapolated to the infinite dilution limit to correct for the concentration effects on the scattering profiles. The corrected profiles were merged with the $S > 0.015$ $Å^{-1}$ profile measured from a 3.2 mg/mL solution. The distance distribution function $P(r)$ was calculated using GNOM (*32*).

The low-resolution molecular models of P2L2K were restored as an assembly of small spheres of 3.8 Å, called dummy residues, using GASBOR (*33*). GASBOR minimizes the discrepancy between experimental and calculated scattering profiles by keeping a compactly interconnected configuration of dummy residues approximating a molecular shape. The discrepancy in the observed and calculated scattering profiles was monitored via the χ^2 value, which is defined as

$$\chi^2 = 1/(N-1)\sum_j \{[c(S_j)I_{exp}(S_j) - KI_{model}(S_j)]/\sigma(S_j)\}^2$$

where N is the number of experimental data points, S_j is the scattering vector of the jth data point, $c(S_j)$ is a correction factor, K is a scale factor, and $\sigma(S_j)$ is the statistical error in the experimental scattering profile $I_{exp}(S_j)$. $I_{model}(S_j)$ represents the scattering profile of the predicted structural model. As GASBOR analysis does not provide a unique solution for three-dimensional structures, 10 independent calculations were performed for a targeted profile, and the obtained molecular models were aligned manually.

Informatics Analysis. To determine which regions of P2L2K were disordered, we calculated the disorder probability of the P2L2K fragment using DISOPRED2 (*34*). Using the Spanner version 1.0.1 server (*35*), structural models of P2LOV2 with the Jα-like region (P2LOV2-Jα, residues 388−529) and P2STK were built against the *Avena* phot1 LOV2 domain in the dark [PDB entry 2V0U (*20*)] and the cAMP-dependent protein kinase in the unliganded state [PDB entry 1J3H (*36*)] as templates, respectively. Ψ-Blast (*37*) was applied to search polypeptides homologous to the linker region with a part of the Jα-like region (residues 508−573) and the activation loop with a 32-residue insertion (*38*) of P2STK (AI-loop, residues 730−556).

RESULTS

Sequence Analysis and Homology Models of P2LOV2, the Linker Region, and P2STK. We first calculated the disorder probability of the P2L2K fragment (Figure 1B). The result indicated that the Jα-like−linker region was likely classified as a naturally unfolded polypeptide that adapted several conformations depending on the interactions with other polypeptide chains (*39*) (Figure 1B). This analysis also revealed that the AI-loop of P2STK appeared to be in an unfolded state to a lesser extent than the linker region. In contrast, small values of disorder probability were observed for P2LOV2, and the N- and C-terminal regions of P2STK supported their naturally folded structure.

The homology models of P2LOV2-Jα and P2STK, with the exception of the AI-loop, displayed nearly identical structures with their corresponding templates (Figure 1C). The root-mean-square differences for Cα atoms between the homology model and its template were 0.3 Å for P2LOV2 and 1.0 Å for P2STK. The Jα-like region was predicted to form a helix resembling the Jα region of the *Avena* phot1 LOV2 domain (*20*, *26*), despite its disorder probability of approximately 0.5. The AI-loop of P2STK appeared in different conformations in each of the calculation runs and showed a high degree of sequence homology with the phosphorylation kinase-inducible domain of the CREB (cyclic AMP response element binding) protein, which displays a coil-to-helix transition upon binding to a domain of the CREB protein (*40*). The homology models of P2LOV2-Jα and P2STK were used to discuss their relative positions in the molecular shape of P2L2K restored from the SAXS profile (see the following sections).

In the Blast search, the Jα-like−linker region displayed E values (*38*) of less than 4.1 against segments in the H-chain of archaeal RNA polymerase [PDB entry 2PMZ (*41*)] and hemoglobin [PDB entry 1GCW (*42*)] (Figure 1D), in addition to the Jα region in *Avena* phot1 LOV2 domain (*20*) and its related proteins. Both segments were judged to be naturally folded by the low disorder probability scores (data not shown). The segment of the H-chain in the RNA polymerase, which had the smallest E value of 0.043 versus the linker region, was composed of a short helix and small antiparallel β-sheet that were connected by several loops. In contrast, the N-terminal half of the hemoglobin segment overlapped with the Jα region of the *Avena* phot1 LOV2 domain, while the C-terminal half was in a helix conformation that was distinct from the homologous region in the RNA polymerase segment.

Spectroscopic Characterization of Purified P2L2K. Following the overexpression and purification of the mutated P2L2K fragment, the SDS−PAGE patterns after the purification (Figure 2A) demonstrated the high purity (>99%) and homogeneity of the prepared P2L2K samples. The mutated P2L2K fragment displayed almost the same responses under blue-light irradiation with nonphosphorylated P2L2K (Figure 2A).

Under blue-light irradiation, P2L2K was then converted to the cysteinyl adduct state (Figure 2A). The amount of P2L2K in the adduct state under successive irradiation increased depending on the fluence rate and reached >95% of P2L2K in the sample over 190 $\mu M\ m^{-2}\ s^{-1}$. The absorption spectra of P2L2K in the dark and adduct states were nearly identical with those of the phot2 LOV2 domain (residues 363−504) and the phot2 LOV2 domain−Jα-like−linker (residues 363−575) fragments, which lacked P2STK (*22*). At a fluence rate of 190 $\mu M\ m^{-2}\ s^{-1}$, adduct formation was saturated within 10 s of the initiation of blue-light illumination. The dark reversion was completed within 2 min of the illumination being turned off, and the observed reversion kinetics were similar to those of the recombinant *Arabidopsis* phot2 LOV2 domain and phot2 LOV2c domain−Jα-like−linker fragments (*22*). Taken together, these findings indicated that P2STK had little influence on the photoreaction cycle of P2LOV2.

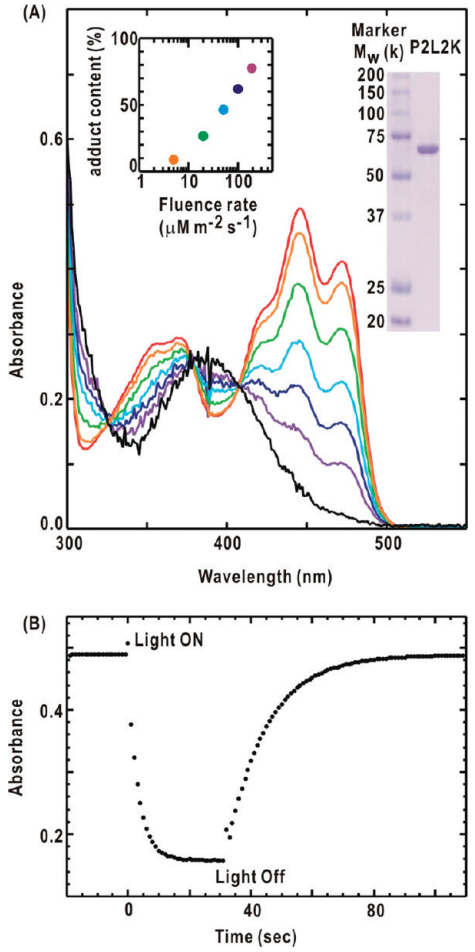

FIGURE 2: (A) Absorption spectra of P2L2K in the dark (solid red line) and under blue-light illumination with fluence rates of 5 (orange), 20 (green), 51 (cyan), 100 (blue), and 190 μM m^{-2} s^{-1} (purple). The black line shows the absorption spectrum of the cysteinyl adduct state (S390) calculated from the variation arising from the fluence rate. The insets at the left show the fluence-dependent formation of the adduct state. The SDS−PAGE pattern at the right demonstrates the purity of the P2L2K samples used in this study. (B) Kinetics of formation of the cysteinyl adduct of P2L2K under blue-light irradiation and reversion in the dark, as monitored by the absorption at 450 nm. The data were taken at a fluence rate of 190 μM m^{-2} s^{-1}.

SAXS Profiles. We next measured SAXS profiles for each P2L2K sample sequentially in the dark (P2L2K$_{dark1}$), under blue-light irradiation (P2L2K$_{light}$), and again in the dark (P2L2K$_{dark2}$). The fluence rate under blue-light irradiation (450 μM m^{-2} s^{-1}) was sufficient for the accumulation of the adduct state as expected from the inset in Figure 2A. The SAXS profiles of P2L2K monotonously decreased to an S of 0.04 Å^{-1} (Figure 3A).

In the concentration range measured, the scattering intensities of P2L2K$_{light}$ decreased from 0.004 to 0.012 Å^{-1} (Figure 3B), while the profiles in the other scattering-angle regions remained unchanged. The decrease in intensity at an S of 0.01 Å^{-1} corresponded to approximately 6% of the intensity of P2L2K$_{dark1}$ at any of the measured concentrations. According to the reciprocity between the scattering vectors and distances of electron pairs within a solute, the changes from 0.004 to 0.012 Å^{-1} suggested that conformational changes occurred among clusters of electron densities separated by ~100 Å. The profiles of P2L2K$_{dark2}$ obtained 5 min after the blue light had been turned off resembled those of P2L2K$_{dark1}$, indicating that the SAXS changes between the dark and light conditions were nearly photoreversible (Figure 3B).

Guinier Analysis. The Guinier plots (*31*) of P2L2K$_{dark1}$, P2L2K$_{light}$, and P2L2K$_{dark2}$ were approximated by straight lines when $S^2 < 40-45 \times 10^{-6}$ Å^{-2} (Figure 3C), and the calculated $C/I(S=0,C)$ and $R_g^2(C)$ values displayed linear concentration dependencies (Figure 3D). These findings indicated that P2L2K$_{dark1}$, P2L2K$_{light}$, and P2L2K$_{dark2}$ solutions possessed monodispersive properties.

The $I(S=0,C)$ values were similar among P2L2K$_{dark1}$, P2L2K$_{light}$, and P2L2K$_{dark2}$, which exhibited small decreases with negative A_2 values (Figure 3D). The apparent M_w values of P2L2K$_{dark1}$, P2L2K$_{light}$, and P2L2K$_{dark2}$ estimated from $I(S=0, C=0)$ demonstrated they existed as a monomeric form in solution (Table 1). Although the $R_g(C=0)$ values differed among the three conditions, the $R_g(C)^2$ displayed concentration dependencies with negative B_{if} values that were nearly identical (Figure 3D and Table 1). The 2.4 Å increase in the $R_g(C=0)$ value of P2L2K$_{light}$ from that of P2L2K$_{dark1}$ (Table 1) was interpreted to mean that the molecular dimension of P2L2K$_{light}$ became larger than that of P2L2K$_{dark1}$. The $R_g(C=0)$ value of P2L2K$_{dark2}$, which was comparable with that of P2L2K$_{dark1}$, suggested that relaxation of the overall structure in the dark proceeded more slowly than that of the FMN moiety in P2LOV2 as monitored by the UV−vis absorption (Figure 2B). The A_2 and B_{if} parameters, which were independent of the light and dark conditions, indicated that the light-induced conformational changes expected from the observed changes in the SAXS profiles (Figure 3B) had little influence on the surface properties of P2L2K.

The $P(r)$ functions of P2L2K$_{dark1}$, P2L2K$_{light}$, and P2L2K$_{dark2}$ had maxima near 40 Å and monotonously decreased to their maximal dimensions (D_{max}) (inset of Figure 3B and Table 1). Differences in the $P(r)$ functions of P2L2K$_{dark1}$ and P2L2K$_{light}$ were prominent at an r of >80 Å, reflecting the extension of the molecular boundary of the P2L2K molecule in P2L2K$_{light}$.

Low-Resolution Molecular Models in the Dark and under Blue-Light Irradiation. The restored molecular models of P2L2K$_{dark1}$, P2L2K$_{light}$, and P2L2K$_{dark2}$ (Figure 4) appeared as elongated shapes and reproduced the experimental profiles (Figure 3A), as indicated by the calculated χ^2 values (Table 1). It should be noted that the mirror images of the molecular models can also explain the measured scattering profiles.

The molecular models of P2L2K$_{dark1}$ and P2L2K$_{dark2}$ almost overlapped and were roughly divided into large and small lobes (the second column in Figure 4A). The large lobe forming the main body of the P2L2K$_{dark1}$ model was approximated as a rectangular plate with rough dimensions of 80 Å (length), 45 Å (width), and 35 Å (thickness), while the ellipsoid-shaped small lobe displayed dimensions of 30 Å (length) and 25 Å (width) and was attached to the edge of the large lobe. Comparison of the sizes and shapes of the homology models (Figure 1C) and the two lobes showed the small lobe was modeled as P2LOV2-Jα and P2STK was assigned to the large lobe (the third column in Figure 4A). In the putatively constructed model, the centers of the two domains were separated by approximately 45 Å, and the molecular boundaries of P2LOV2-Jα and the N-domain of P2STK were in slight contact. The linker region was assumed to occupy the space between P2LOV2-Jα and P2STK in the restored models.

The molecular model of P2L2K$_{light}$ appeared as a more extended shape than those of the dark state (the second column of Figure 4B). Overlapping of the main bodies of the P2L2K$_{light}$ and

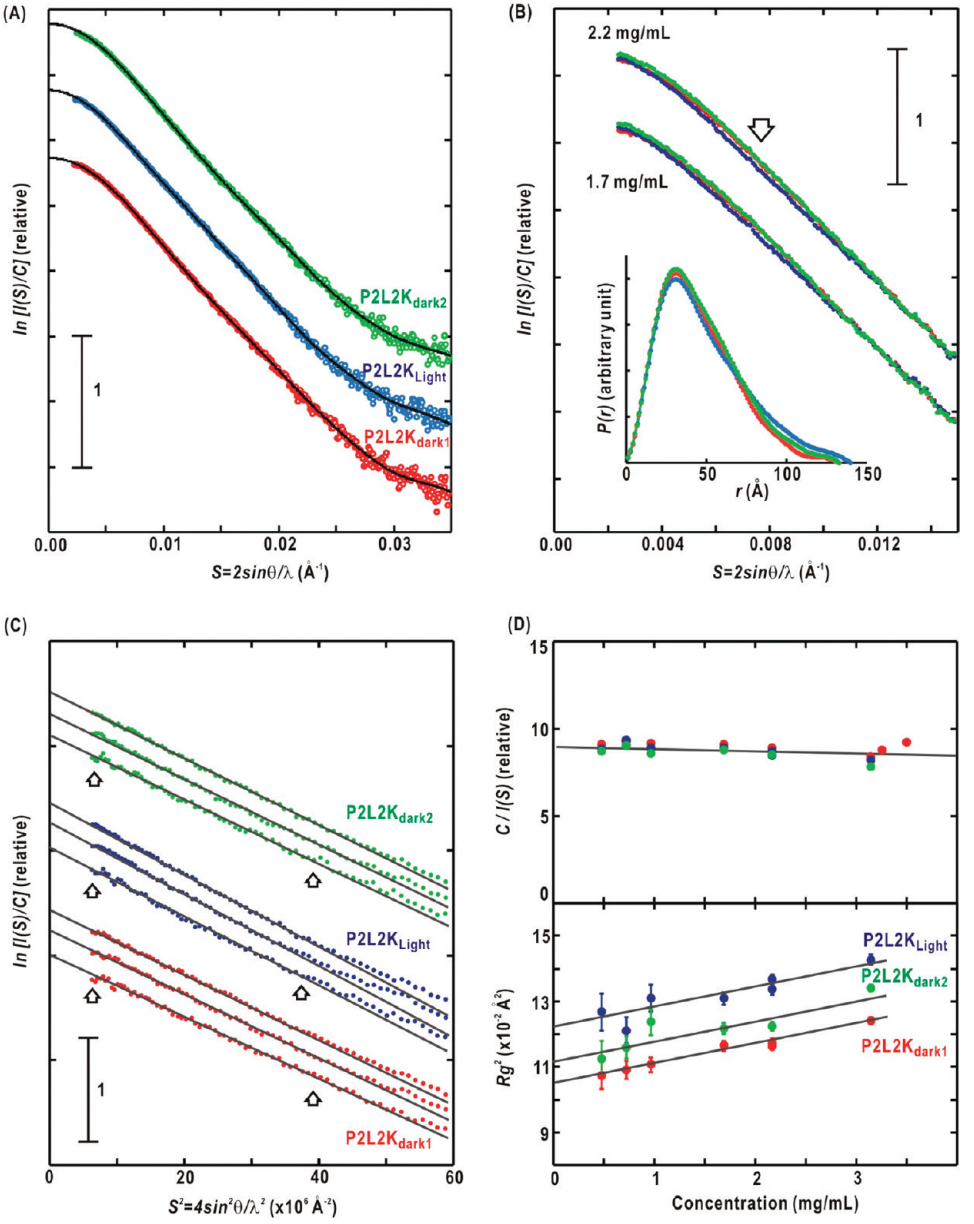

FIGURE 3: (A) SAXS profiles of P2L2K$_{dark1}$ (red), P2L2K$_{light}$ (blue), and P2L2K$_{dark2}$ (green) at the dilution limit. The scattering intensities are plotted in semilogarithmic form and are shifted appropriately along the ordinate for the sake of clarity. The black lines are profiles of the predicted structural models from GASBOR (*33*). (B) Comparison of scattering profiles of P2L2K$_{dark1}$ (red), P2L2K$_{light}$ (blue), and P2L2K$_{dark2}$ (green) at two different concentrations (1.7 and 2.2 mg/mL). The data sets are shifted appropriately along the ordinate for the sake of clarity. The arrow indicates the region in which intensity changes are the most prominent between P2L2K$_{light}$ and P2L2K$_{dark1}$. The inset compares the $P(r)$ functions of P2L2K$_{dark1}$ (red), P2L2K$_{light}$ (blue), and P2L2K$_{dark2}$ (green). (C) Guinier plots, which represent the logarithm of scattering intensities plotted vs the square of the scattering vector, of P2L2K$_{dark1}$ (red), P2L2K$_{light}$ (blue), and P2L2K$_{dark2}$ (green). Under each condition, the concentrations of sample solutions are 1.0, 1.7, and 2.2 mg/mL from top to bottom. The data are shifted appropriately along the ordinate for the sake of clarity. The regions used for the Guinier approximations in panel D are denoted with a pair of arrows. The black lines were calculated by the least-squares method for the arrowed regions. The high-angle edges of the regions satisfy the criteria for the approximation [$SR_g < (2\pi)^{-1}$]. (D) Concentration dependencies of $C/I(0,C)$ (top) and $R_g(C)^2$ (bottom) of P2L2K$_{dark1}$ (red), P2L2K$_{light}$ (blue), and P2L2K$_{dark2}$ (green), showing the standard deviation values. With regard to the data for $C/I(0,C)$, the standard deviations are within the symbols. The black regression lines were calculated by the least-squares method.

P2L2K$_{dark1}$ models revealed that the small lobe of P2L2K$_{light}$ was approximately 1.2-fold longer than that of P2L2K$_{dark1}$. When the P2LOV2-Jα model was set at the center of the small lobe, it shifted approximately 13 Å from the position in P2L2K$_{dark1}$ with a slight inclination of the molecular axis. The positional shift of P2LOV2-Jα was thought to be a major cause of the increase in the $R_g(0)$ value in P2L2K$_{light}$ (Table 1). The comparison of the molecular models of P2L2K$_{dark1}$, P2L2K$_{light}$, and P2L2K$_{dark2}$ suggested a light-dependent and photoreversible movement of P2LOV2-Jα relative to P2STK.

The P2STK region of the SAXS models resembled the crystal structures of Tyr and Ser/Thr kinases, including c-Fes tyrosine kinase (Fes) (*43*) and C-terminal Src kinase (Csk) in their inactive and active forms (*44*), anti-Ca/CaM kinase II-a-Subunit (c-Abl) in the activated form (*45*), and Rio2 serine kinase (Rio2) (*46*) (Figure 5). When the crystal structures of these protein kinases were superimposed on the P2L2K$_{dark}$ model, their regulatory domains occupied the space assigned as the linker region of P2L2K. In contrast, the P2L2K model differed from the crystal structures of c-Abl (*47*), c-Src (*48*), and Hck (*49*) Tyr kinases in their autoinhibited

Table 1: Molecular Weights and Structural Parameters of P2L2K

state	$I(0,0)$	SAXS M_w[a]	$R_g(0)$ (Å)	D_{max} (Å)[b]	χ^2 of models[b]
$P2L2K_{dark1}$	110	57.6K	32.4 ± 0.4	133 ± 2	1.6
$P2L2K_{light}$	112	58.4K	34.8 ± 0.7	140 ± 2	1.5
$P2L2K_{dark2}$	114	59.6K	33.4 ± 0.5	133 ± 2	1.6

[a]The calculated M_w of P2L2K from the amino acid sequence was 62.4K. [b]The χ^2 values represent the average of 10 independent GASBOR (*33*) calculations.

form. In the crystal structures, the regulatory domains associated with the kinase domains at sites distal from the active site cleft. The $P2L2K_{dark}$ model was also different from the crystal structure of protein kinase A (PKA) in complex with its regulatory subunit RIα, which associated with the active site of PKA (*50*).

DISCUSSION

This study demonstrates the occurrence of light-dependent changes in the SAXS profiles (Figure 3) of monomeric P2L2K containing the Asp720Asn mutation (Figure 2). The observed SAXS changes suggested a photoreversible movement of P2LOV2-Jα relative to P2STK (Figure 4). On the basis of the SAXS data and homology models of the P2L2K functional domains, here, we discuss the possible molecular mechanisms that would explain the light-dependent conformational changes in P2L2K (Figures 3 and 4). As the obtained SAXS models displayed similar shapes with the kinase proteins shown in Figure 5, the activation mechanisms in these kinase proteins may provide clues for our understanding of the intramolecular propagation of conformational changes within P2L2K.

Ser/Thr and Tyr kinases, which display conformational plasticity (*51*), contain regulatory domains that probably play essential roles in stabilizing the structure of kinase domains and prolonging the activated state (*52*). Through comparisons of their crystal structures in the active and autoinhibited/inactive forms, several types of activation mechanisms for kinase domains have been proposed. For instance, the Src homology 2 (SH2) and Src homology 3 (SH3) domains in the activated forms of c-Abl and Src travel approximately 70 Å from their positions in the autoinhibited forms to realize the interactions between the SH2 domain and N-terminal region of the kinase domain, which are indispensable for the activity of the kinase domain (*45*, *47*, *53*). In addition, the movement of the stimulated SH2 domains in Csk and Fes is necessary to structurally stabilize the N-terminal lobe of the kinase domain (*43*, *44*, *54*). These facts suggest that intramolecular signals are transmitted through interactions between the regulatory and kinase domains.

In P2L2K, the light-induced conformational changes in P2LOV2 are assumed to be minor in referring to the conformational changes observed in the LOV2 core of *Avena* phot1 (*20*, *26*), and the Asp720Asn mutant P2STK, which lacks the affinity for Mg-ATP, will display also small conformational fluctuations as observed in the SAXS analysis on the unliganded kinase domain from c-Abl (*45*). Thus, specifically, as the regulatory domains of several kinase proteins occupy the space assigned to the linker region in the P2L2K SAXS model (Figure 5), the region located at the P2LOV2−P2STK interface, probably including the linker and a part of the Jα-like regions displaying large disorder probabilities (Figure 1B), likely plays a key role in the interdomain signal transduction in P2L2K.

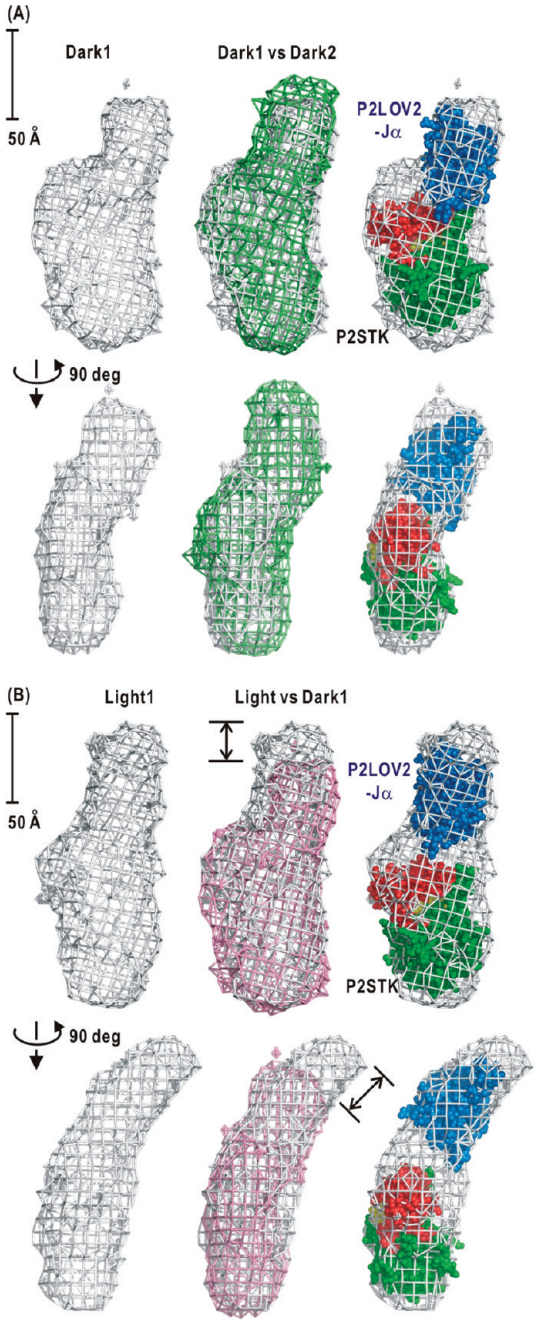

FIGURE 4: Molecular models restored from SAXS profiles for $P2L2K_{dark1}$ (A) and $P2L2K_{light}$ (B). The molecular models in the first column are shown as density maps of dummy residues (gray mesh) in 4 Å × 4 Å × 4 Å cubes after the independent superimposition of 10 restored models. The second row in each panel illustrates the models rotated 90° around their molecular axis from those in the first row. The second column in panel A compares the $P2L2K_{dark1}$ and $P2L2K_{dark2}$ (green mesh) models, and that in panel B compares $P2L2K_{light}$ and $P2L2K_{dark1}$ (pink). The third column in panels A and B illustrates the P2LOV2-Jα and P2STK homology models (shown by the space-filling atoms colored as in Figure 1C) putatively fitted to the molecular models of $P2L2K_{dark1}$ and $P2L2K_{light}$. The P2LOV2-Jα and P2STK models were set so that the N-terminal domain of P2STK faced the C-terminal region of P2LOV2-Jα. When the C-terminal domain of P2STK was set near the P2LOV2-Jα C-terminal region, it was difficult to connect them with the linker region, even in its extended conformation. The molecular models in this figure were prepared using PyMol (*56*).

In this regard, our previous SAXS study provides insight into the flexibility of the linker region, which is predicted to be a

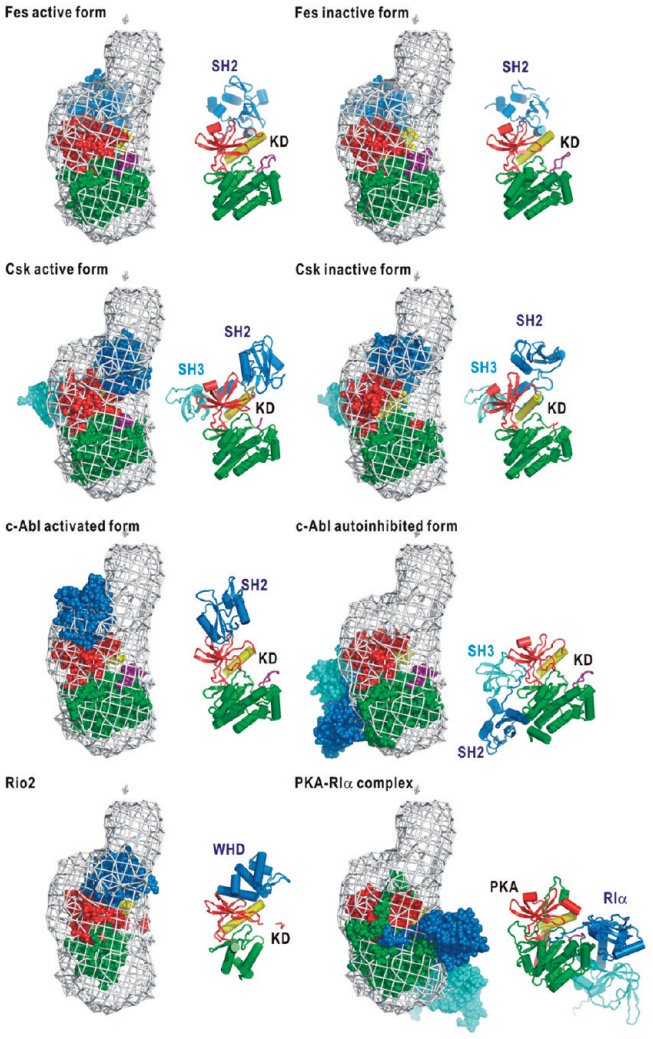

FIGURE 5: Comparison of the SAXS model for P2L2K$_{dark1}$ (gray) with the crystal structures of selected Tyr and Ser/Thr protein kinases. The crystal structures of Fes (*43*) and Csk (*44*) in active and inactive forms, c-Abl in activated (*45*) and autoinhibited (*47*) forms, Rio2 (*46*), and PKA-RI (*50*) were compared. Kinase domains (KDs) are colored as in Figure 1. Purple-colored segments represent the A-loop, while the regulatory domains and subunits [SH2, SH3, winged-helix domains (WHD), and RIα] are colored blue or cyan. The molecular models in this figure were prepared using PyMol (*56*).

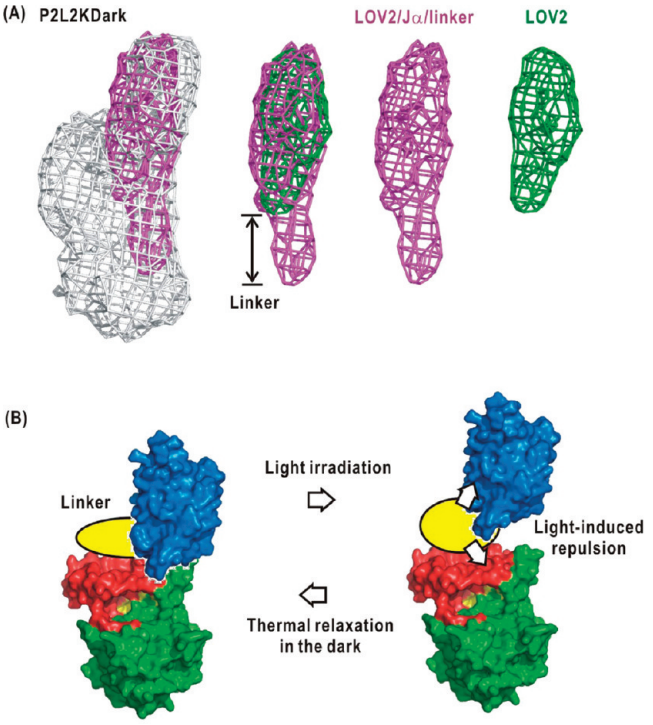

FIGURE 6: (A) Comparison of the SAXS models of P2L2K$_{dark1}$ (gray), phot2 LOV2 domain (green), and phot2 LOV2 domain−Jα−linker (purple) fragments. The models for phot2 LOV2 domain and phot2 LOV2 domain−Jα−linker fragments were taken from our previous SAXS study (*22*). The models are shown as in Figure 4. (B) Schematic illustration explaining the light-induced conformational changes that occur in P2L2K. The colors of the domains are as in Figure 1, and the linker is drawn with a yellow circle. This figure was prepared using PyMol (*56*).

naturally unfolded polypeptide (Figure 1B,D). From the SAXS of a recombinant phot2 LOV2 domain−Jα−linker fragment (residues 363−575), we obtained an elongated shape with a characteristic extension of approximately 40 Å that was assumed to be the linker region (*22*). When the phot2 LOV2 domain−Jα−linker and P2L2K$_{dark1}$ models were superimposed so that their P2LOV2 regions overlapped optimally, the linker region of the fragment overlapped with the P2STK portion in the P2L2K$_{dark}$ model (Figure 6A). This comparison implies that the linker region exposed to bulk solvent folds into a conformation different from that in P2L2K because of the absence of interactions with P2STK.

The blue-light-triggered unfolding and/or conformational changes of the Jα helix are suggested from reported spectroscopic measurements for the *Avena* phot1 LOV2 domain and *Arabidopsis* phot2 LOV2 domain (*26*−*28*). While the overall restored molecular shape can be discussed with regard to the arrangements of the domains from our SAXS data at a resolution of 25 Å (S = 0.04 Å^{-1}) (Figure 4), it is difficult to speculate about the light-induced structural changes of the Jα-like region (Figures 1C and 4). However, the conformational changes expected in the linker region suggested in the SAXS models (Figure 4) may be relevant to the observations in the spectroscopic studies.

Thus, in P2L2K, the Jα-like and linker regions are thought to display conformational changes through adapting to the small external perturbation from photoactivated P2LOV2. The conformational changes would result in the separation of P2LOV2 and P2STK and also serve to rearrange the segments controlling the conformation of the active site cleft in P2STK (Figure 6B). Notably, the structural changes have little influence on the overall surface properties of P2L2K, as indicated by the SAXS parameters (Figure 3D). An in vitro assay has suggested that the *Arabidopsis* phot2 LOV2 and kinase domains associate in the dark and dissociate under blue-light illumination (*24*). The scheme for the light-induced conformational changes in P2L2K described above may be relevant for the results of the in vitro assays.

This scheme for the intramolecular signal transduction from the photoactivated P2LOV2 to P2STK, however, is inconsistent with that proposed previously (*55*). According to the previous scheme, P2LOV2 under dark conditions is thought to directly associate with the active site cleft of P2STK as observed in the association of the RIα segment with PKA (*50*), and P2LOV2 is expected to dissociate from P2STK upon light irradiation. The scheme is proposed on the basis of the sequence similarity between the Fα helix of P2LOV2 and an inhibitor polypeptide for PKA and is now being used to interpret the results from the spectroscopic measurements of algal phototropin (*29*). To clarify

whether P2LOV2 binds to the active site of P2STK in nonphosphorylated wild-type P2L2K, the influences of the Asp720Asn mutation on the structure of P2L2K remain to be investigated in the next stage of our research. In addition, we are constructing mutants that include the Cys426Ala mutation to identify residues involved in the transmission of the blue-light-induced conformational change from P2LOV2 to P2STK.

Finally, we here mention the quaternary structure of full-length *Arabidopsis* phot2. In the previous studies, we demonstrated the dimeric association of the LOV1 domain (residues 117−265) of *Arabidopsis* phot2 both in solution (*22*) and in the crystal (*23*) and the monomeric state of the LOV2 domain and the LOV2 domain−Jα−linker fragment in solution (*22*). This SAXS study suggests the monomeric state of P2L2K (Figures 3 and 4). Thus, although the structural information is still limited in vitro, full-length phot2 is expected to be dimerized at the LOV1 domain, and the two P2L2K regions in the dimer are almost free from mutual contacts as suggested by the SAXS parameters (Figure 3D and Table 1). It is interesting to study whether the quaternary structure of phot2 is relevant to the fluence rate-dependent responses of phot2 in vivo.

ACKNOWLEDGMENT

We thank Prof. Masaki Yamamoto and Dr. Takaaki Hikima of the RIKEN Harima Institute for their kind help with the SAXS experiments at BL45XU of SPring-8. We are grateful to Dr. Greg Newton for his kind suggestions in editing our manuscript. The SAXS experiments were conducted under the approval of the RIKEN Harima Institute.

SUPPORTING INFORMATION AVAILABLE

SAXS experiments on P2L2K solutions with and without ultracentrifugation. This material is available free of charge via the Internet at http://pubs.acs.org.

REFERENCES

1. Quail, P. H. (2002) Photosensory perception and signaling in plant cells: New paradigms? *Curr. Opin. Cell Biol. 140*, 180–188.
2. Chen, M., Chory, J., and Fankhauser, C. (2004) Light signal transduction in higher plants. *Annu. Rev. Genet. 38*, 87–117.
3. Briggs, W. R., and Christie, J. M. (2002) Phototropins 1 and 2: Versatile plant blue-light receptors. *Trends Plant Sci. 7*, 204–210.
4. Christie, J. M. (2007) Phototropin blue-light receptors. *Annu. Rev. Plant Biol. 58*, 21–45.
5. Christie, J. M., Reymond, P., Powell, G. K., Bernasconi, P., Raibekas, A., Liscum, E., and Briggs, W. R. (1998) *Arabidopsis* NPH1: A flavoprotein with the properties of a photoreceptor for phototropism. *Science 282*, 1698–1701.
6. Jarillo, G. A., Gabrys, H., Capel, J., Alonso, J. M., Ecker, J. R., and Cashmore, A. R. (2001) Phototropin-related NPL1 controls chloroplast relocation induced by blue light. *Nature 410*, 952–954.
7. Kagawa, T., Sakai, T., Suetsugu, N., Oikawa, K., Ishiguro, S., Kato, T., Tabata, S., Okada, K., and Wada, M. (2001) *Arabidopsis* NPL1: A phototropin homolog controlling the chloroplast high-light avoidance response. *Science 291*, 2138–2141.
8. Sakai, T., Kagawa, T., Kasahara, M., Swartz, T., Christie, J. M., Briggs, W. R., Wada, M., and Okada, K. (2001) Photochemical properties of the flavin mononucleotide-binding domains of the phototropins from *Arabidopsis*, Rice, and *Chlamydomonas reinhardtii*. *Proc. Natl. Acad. Sci. U.S.A. 98*, 6969–6974.
9. Kinoshita, T., Doi, M., Suetsugu, N., Kagawa, T., Wada, M., and Shimazaki, K. (2001) Phot1 and phot2 mediate blue light regulation of stomatal opening. *Nature 414*, 656–660.
10. Briggs, W. R., Beck, C., Cashmore, A. R., Christie, J. M., Hughes, J., Jarillo, J. A., Kagawa, T., Kanegae, H., Liscum, E., Nagatani, A., Okada, K., Salomon, M., Rüdiger, W., Sakai, T., Takano, M., Wada, M., and Watson, J. C. (2001) The phototropin family of photoreceptors. *Plant Cell 13*, 993–997.
11. Cheng, P., He, Q., Yang, Y., Wang, L., and Liu, Y. (2003) Functional conservation of light, oxygen, or voltage domains in light sensing. *Proc. Natl. Acad. Sci. U.S.A. 100*, 5938–5943.
12. Crosson, S., and Moffat, K. (2001) Structure of a flavin-binding plant photoreceptor domain: Insights into ligand-mediated signal transduction. *Proc. Natl. Acad. Sci. U.S.A. 98*, 2995–3000.
13. Taylor, B. L., and Zhulin, I. B. (1999) PAS domains: Internal sensors of oxygen, redox potential and light. *Microbiol. Mol. Biol. Rev. 63*, 479–506.
14. Bogre, L., Okresz, L., Henriques, R., and Anthony, R. G. (2003) Growth signaling pathway in *Arabidopsis* and the AGC protein kinases. *Trends Plant Sci. 8*, 424–432.
15. Inoue, S., Kinoshita, T., Matsuomoto, M., Nakayama, K. I., Doi, M., and Shimazaki, K. (2008) Blue light-induced autophosphorylation of phototropin is a primary step for signaling. *Proc. Natl. Acad. Sci. U.S.A. 105*, 5626–5631.
16. Sullivan, S., Thomson, C. E., Lamont, D. J., Jones, M. A., and Christie, J. M. (2008) In vivo phosphorylation site mapping and functional characterization of *Arabidopsis* phototropin 1. *Mol. Plant 1*, 178–194.
17. Salomon, M., Christie, J. M., Kneib, E., Lempert, U., and Briggs, W. R. (2000) Photochemical and mutational analysis of the FMN-binding domains of the plant blue light receptor, phototropin. *Biochemistry 39*, 9401–9410.
18. Swartz, T. E., Corchnoy, S. B., Christie, J. M., Lewis, J. W., Szundi, I., Briggs, W. R., and Bogomolni, R. A. (2001) The photocycle of a flavin-binding domain of the blue light photoreceptor phototropin. *J. Biol. Chem. 276*, 36493–36500.
19. Crosson, S., and Moffat, K. (2002) Photoexcited structure of a plant photoreceptor domain reveals a light-driven molecular switch. *Plant Cell 14*, 1067–1075.
20. Halavaty, A. S., and Moffat, K. (2007) N- and C-Terminal flanking regions modulate light-induced signal transduction in the LOV2 domain of the blue light sensor phototropin 1 from *Avena sativa*. *Biochemistry 46*, 14001–14009.
21. Christie, J. M., Swartz, T. E., Bogomolni, R. A., and Briggs, W. R. (2002) Phototropin LOV domains exhibit distinct roles in regulating photoreceptor function. *Plant J. 32*, 205–219.
22. Nakasako, M., Iwata, T., Matsuoka, D., and Tokutomi, S. (2004) Light-induced structural changes of LOV-domain containing polypeptides from *Arabidopsis* phototropin 1 and 2 studied by small-angle X-ray scattering. *Biochemistry 43*, 14881–14890.
23. Nakasako, M., Zikihara, K., Mtsuoka, D., Katsura, H., and Tokutomi, S. (2008) Structural Basis of the LOV1 Dimerization of *Arabidopsis* Phototropins 1 and 2. *J. Mol. Biol. 381*, 718–733.
24. Matsuoka, D., and Tokutomi, S. (2005) Blue light-regulated molecular switch of Ser/Thr kinase in phototropin. *Proc. Natl. Acad. Sci. U.S.A. 102*, 13337–13342.
25. Cho, H.-Y., Tseng, T.-S., Kaiserli, E., Sullivan, S., Christie, J. M., and Briggs, W. R. (2007) Physiological roles of the light, oxygen, or voltage domains of phototropin 1 and phototropin 2 in *Arabidopsis*. *Plant Physiol. 143*, 517–529.
26. Harper, S. M., Neil, L. C., and Gardner, K. H. (2003) Structural basis of a phototropin light switch. *Science 301*, 1541–1544.
27. Chen, E., Swartz, T. E., Bogomolni, R. A., and Kliger, D. S. (2007) A LOV story: The signaling state of the phot1 LOV2 photocycle involves chromophore-triggered protein structure relaxation, as probed by far-UV time-resolved optical rotatory dispersion spectroscopy. *Biochemistry 46*, 4619–4624.
28. Eitoku, T., Nakasone, Y., Zikihara, K., matsuoka, D., Tokutomi, S., and Terazima, M. (2007) Photochemical intermediates of *Arabidopsis* phototropin 2 LOV domains associated with conformational changes. *J. Mol. Biol. 371*, 1290–1303.
29. Pfeifer, A., Mathes, T., Lu, Y., Hegemann, P., and Kottke, T. (2010) Blue light induces global and localized conformational changes in the kinase domain of full-length phototropin. *Biochemistry 49*, 1024–1032.
30. Nakasako, M., Iwata, T., Inoue, K., and Tokutomi, S. (2005) Light-induced global structural changes in phytochrome A regulating photomorphogenesis in plants. *FEBS J. 272*, 603–612.
31. Guinier, A., and Fournet, G. (1955) Small-Angle Scattering of X-rays, John Wiley, New York.
32. Svergun, D. I. (1992) Determination of the regularization parameter in indirect-transform methods using perceptual criteria. *J. Appl. Crystallogr. 25*, 495–503.
33. Svergun, D. I., Petoukhov, M. V., and Koch, M. H. J. (2001) Determination of domain structure of proteins from X-ray solution scattering. *Biophys. J. 80*, 2946–2953.
34. Ward, J. J., Sodhi, J. S., McGuffin, L. J., Buxton, B. F., and Jones, D. T. (2004) Prediction and functional analysis of native disorder in proteins from the three kingdoms of life. *J. Mol. Biol. 337*, 635–645.

35. Lis, M., Standley, D. M., and Nakamura, H. (2010) Hybrid template modeling Spanner version 1.0.1, PDBj, Osaka University, Japan (http://sysimm.ifrec.osaka-u.ac.jp/cgi-bin/spanner).
36. Akamine, P., Madhusudan, Wu. J., Xuong, N.-H., Ten Eyck, L. F., and Taylor, S. S. (2003) Dynamic features of cAMP-dependent protein kinase revealed by apoenzyme crystal structure. *J. Mol. Biol. 327*, 159–171.
37. Altschul, S. F., Madden, T. L., Schäffer, A. A., Zhang, J., Zhang, Z., Miller, W., and Lipman, D. J. (1997) Gapped BLAST and PSI-BLAST: A new generation of protein database search program. *Nucleic Acids Res. 25*, 3389–3402.
38. Matsuoka, D., Iwata, T., Zikihara, K., Kandori, H., and Tokutomi, S. (2007) Primary processes during the light-signal transduction of phototropin. *Photochem. Photobiol. 83*, 122–130.
39. Wright, P. E., and Dyson, H. J. (1999) Intrinsically unstructured proteins: Re-assessing the protein structure-function paradigm. *J. Mol. Biol. 293*, 321–331.
40. Radhakrishnan, I., Pérez-Alvarado, G. C., Paker, D., Dyson, H. J., Montminy, M. R., and Wright, P. E. (1997) Solution structure of the KIX domain of CBP bound to the transactivation domain of CREB: A model for activator:coactivator interactions. *Cell 91*, 741–752.
41. Hirata, A., Klein, B. J., and Murakami, K. S. (2008) The X-ray crystal structure of RNA polymerase from archaea. *Nature 451*, 851–854.
42. Naoi, Y., Chong, K.-T., Yoshimatsu, K., Miyazaki, G., Tame, J. R., Park, S.-Y., Adachi, S., and Morimoto, H. (2001) The functional similarity and structural diversity of human and cartilaginous fish hemoglobins. *J. Mol. Biol. 307*, 259–270.
43. Filippakopoulos, P., Kofler, M., Hantschel, O., Gish, G. D., Grebien, F., Salah, E., Neudecker, P., Kay, L. E., Turk, B. E., Superti-Furga, G., Pawson, T., and Knapp, S. (2008) Structural coupling of SH2-kinase domains links Fes and Abl substrate recognition and kinase activation. *Cell 134*, 793–803.
44. Ogawa, A., Takayama, Y., Sakai, H., Chong, K. T., Takeuchi, S., Nakagawa, A., Nada, S., Okada, M., and Tsukihara, T. (2002) Structure of the carboxyl-terminal Src kinase, Csk. *J. Biol. Chem. 277*, 14351–14354.
45. Nagar, B., Hantschel, O., Seeliger, M., Davies, J. M., Weis, W. I., Superti-Furga, G., and Kuriyan, J. (2006) Organization of the SH3-SH2 unit in active and inactive forms of the c-Abl tyrosine kinase. *Mol. Cell 21*, 787–798.
46. LaRonde-LeBlanc, N., and Wlodawer, A. (2004) Crystal structure of *A. fulgidus* Rio2 defines a new family of serine protein kinases. *Structure 12*, 1585–1594.
47. Nagar, B., Hantschel, O., Young, M. A., Scheffzek, K., Veach, D., Bornmann, W., Clarkson, B., Superti-Furga, G., and Kuriyan, J. (2003) Structural basis for autoinhibition of c-Abl tyrosine kinase. *Cell 112*, 859–871.
48. Xu, W., Harrison, S. C., and Eck, M. J. (1997) Three-dimensional structure of the tyrosine kinase c-Src. *Nature 385*, 595–602.
49. Sicheri, F., Moarefi, I., and Kuriyan, J. (1997) Crystal structure of the Scr-family tyrosine kinase Hck. *Nature 385*, 602–609.
50. Kim, C., Cheng, C. Y., Saldanha, S. A., and Taylor, S. S. (2007) PKA-I holoenzyme structure reveals a mechanism for cAMP-dependent activation. *Cell 130*, 1032–1043.
51. Huse, M., and Kuriyan, J. (2002) The conformational plasticity of protein kinase. *Cell 109*, 275–282.
52. Ubersax, J. A., and Ferrell, J. E., Jr. (2007) Mechanism of specificity in protein phosphorylation. *Nat. Rev. Mol. Cell Biol. 8*, 530–541.
53. Bernadó, P., Pérez, Y., Svergun, D. I., and Pons, M. (2008) Structural characterization of the active and inactive states of Src kinase in solution by small-angle X-ray scattering. *J. Mol. Biol. 376*, 492–505.
54. Mikkola, E. T., and Gahmberg, C. G. (2010) Hydrophobic interaction between the SH2 domain and the kinase domain is required for the activation of Csk. *J. Mol. Biol. 399*, 618–627.
55. Tokutomi, S., Matsuoka, D., and Zikihara, K. (2008) Molecular structure and regulation of phototropin kinase by blue light. *Biochim. Biophys. Acta 1784*, 133–142.
56. DeLano, W. L. (2002) The PyMol Molecular Graphics System, DeLano Scientific, Palo Alto, CA.